Lensless phase contrast microscopy based on multiwavelength Fresnel diffraction

Daniel W. E. Noom, Kjeld S. E. Eikema, and Stefan Witte*

LaserLaB, Department of Physics and Astronomy, VU University Amsterdam, De Boelelaan 1081, 1081 HV Amsterdam, The Netherlands

**Corresponding author: stefan.witte@vu.nl*

Received October 29, 2013; accepted November 15, 2013;
posted November 27, 2013 (Doc. ID 200371); published January 3, 2014

We demonstrate a compact, wide-field, quantitative phase contrast microscope that does not require lenses for image formation. High-resolution images are retrieved from Fresnel diffraction patterns recorded at multiple wavelengths, combined with a robust iterative phase retrieval algorithm. Quantitative phase contrast images of living cultured neurons are obtained with a transverse resolution of <2 μm. Our system is well suited for high-resolution live cell imaging and provides a compact, cost-effective alternative to full-sized phase-contrast microscopes.

OCIS codes: (180.0180) Microscopy; (100.5070) Phase retrieval; (170.3880) Medical and biological imaging; (110.1650) Coherence imaging.

http://dx.doi.org/10.1364/OL.39.000193

Ever since its invention, microscopy has been an essential technology in life science research. Microscope development has seen tremendous improvements, resulting in advanced approaches, such as multiphoton microscopy [1] and superresolution imaging [2,3]. In many cases, there is a need to record images of living cells with a compact and/or cost-effective device. Such a situation occurs for instance in cases where space or environmental constraints make the use of a full-size microscope challenging. Furthermore, compact, robust, and therefore easily transportable devices may provide a solution for clinical diagnostics in remote areas, or to reduce health care costs by providing low-cost imaging tools for point-of-care diagnostics. Since the main factor that determines both cost and size of a microscope is usually the imaging optics, a significant step toward a compact device can be expected if the imaging can be performed without lenses. In practice, this means that the effects of wave propagation and diffraction need to be overcome in a different way. A variety of solutions to this challenge have been reported. These include minimization of the sample-camera distance by growing cells directly on a CMOS sensor [4], in-line holographic methods [5,6], and numerical reconstruction of an image from a coherent diffraction pattern [7,8].

Here we demonstrate a compact, high-resolution lensless microscope, which can image complex (i.e., modulating both phase and amplitude of the incident field), extended objects without requiring any *a priori* knowledge of the sample itself. The microscope does not contain any moving parts, and only uses commercially available diode lasers and a CCD sensor. To obtain an image, we record Fresnel diffraction patterns of the sample at multiple wavelengths, and use these patterns as input in an iterative phase-retrieval algorithm. After retrieving the phase of the diffraction patterns, numerical backpropagation results in a near-diffraction-limited image of the illuminated object. This approach provides quantitative phase contrast images of the sample, making it ideally suited for live cell imaging studies.

In the near-field regime, the propagation of an electromagnetic field distribution over a distance z can be described by the Fresnel diffraction integral:

$$E(x,y,z) = \frac{e^{i2\pi z/\lambda}}{i\lambda z}\iint E(x',y',0)e^{\frac{i\pi}{\lambda z}[(x-x')^2+(y-y')^2]}\mathrm{d}x'\mathrm{d}y'. \tag{1}$$

To enable backpropagation of a recorded diffraction pattern to the object plane, the phase associated with this diffraction pattern needs to be retrieved through numerical means. Both in-line holographic reconstruction and Gerchberg–Saxton-based iterative algorithms have been applied to this end, although these methods are usually limited in their abilities by the fact that only a single diffraction pattern is recorded. Iterative phase retrieval algorithms rely on propagation to couple amplitude and phase, and therefore require some knowledge at an additional position besides the measurement plane. This introduces the need for support constraints in the object plane [7,9]. Such constraints can be circumvented if multiple measurements are taken under different propagation conditions, e.g., by recording diffraction patterns at multiple distances from an object [10–12]. However, this approach requires either sample or camera movement, making it slow and sensitive to transverse displacements. Ptychography is an approach that uses multiple images that are transversely displaced from each other to introduce redundancy and enable robust phase retrieval [13–15], although a large set of diffraction patterns needs to be recorded. Alternatively, we show that diffraction patterns at a single position but with multiple wavelengths can also be used as input for iterative phase retrieval. A major advantage of this "wavelength diversity" approach is that no moving parts are needed, while still allowing robust phase retrieval even with complex, extended samples. Wavelength-dependent diffraction of incoherent light has recently also been exploited in wide-field and fluorescence microscopes for imaging of several axial planes simultaneously [16]. We have

recently implemented this approach to facilitate imaging at extreme-ultraviolet wavelengths, using spectrally resolved input images from a Fourier-transform-based two-pulse lensless imaging scheme [17]. When using visible light, it allows microscopy with a highly compact and simple setup, and allows for fast image acquisition.

To retrieve an image of an object, we record a diffraction pattern of that object at either two or three different wavelengths. These diffraction patterns are used as input in an iterative phase retrieval algorithm, in which we start with a single diffraction pattern at wavelength λ_1 with a random phase, and "propagate" this field numerically to the second wavelength λ_2. After propagation, we retain the phase but replace the amplitude by the actually measured amplitude at λ_2, and propagate back to λ_1 (or onward to a third wavelength). To propagate the diffraction pattern from λ_1 to λ_2, we first propagate to the object plane by Fourier transformation, multiplication with the free-space propagation transfer function [18]:

$$H(f_x,f_y,\lambda_1) = e^{i2\pi z\sqrt{\frac{1}{\lambda_1^2}-f_x^2-f_y^2}}, \tag{2}$$

and inverse Fourier transformation. In Eq. (2), f_x and f_y are the spatial frequencies along the x- and y-axis, respectively. At the object plane, we divide the phase pattern by the wavelength ratio λ_2/λ_1 to account for the difference in phase shift that the object introduces for different wavelengths, and subsequently propagate back from the object plane using the conjugate propagation transfer function $H^*(f_x,f_y,\lambda_2)$. This calculation is more general than the Fresnel propagation Eq. (1), as it is not restricted to small angles. The algorithm typically requires 10–40 iterations over all wavelengths to converge to a final solution for the phase. The retrieved field is then propagated back to the object plane to recover the exit surface wave, which is the product of the illumination function and the complex object transmission function. As the illumination is a smooth Gaussian profile, a clear image of the object is readily obtained. Both the amplitude and phase are retrieved, providing a bright-field and a quantitative phase contrast image simultaneously.

A schematic of the lensless microscope is shown in Fig. 1(a). We use three diode lasers at wavelengths of 685, 785, and 940 nm, butt-coupled to single-mode fibers (SMFs). The laser outputs are combined by broadband 2×2 fiber beam splitters, resulting in an alignment-free light source where all three wavelengths are emitted by a SMF, ensuring perfect spatial overlap and spatial coherence. The light emanating from the fiber output is directly sent onto the sample, and a CCD camera (AVT Prosilica GC1920, 14 bits, 1936×1456 pixels, 4.54 μm pixel size) records the resulting diffraction patterns. We acquire diffraction patterns at each of the three wavelengths consecutively by sequentially switching the lasers on and off.

As a first test we perform imaging of a USAF 1951 test target in transmission. The fiber output is placed at a distance of 1.2 mm in front of the object, and the CCD is placed at 9 mm behind the object. This results in a NA of 0.36 for detection of the diffracted light (determined by the size of the CCD sensor), which would allow a diffraction-limited resolution of 1.2 μm. The field-of-view

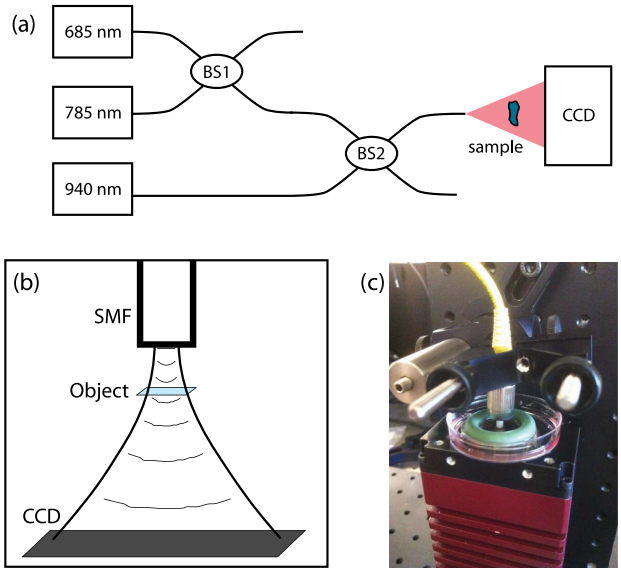

Fig. 1. (a) Schematic of the all-fiber-based lensless imaging setup. Three fiber-coupled laser diodes are combined into a single fiber using 2×2 fiber beam splitters (BS1 and BS2). The fiber output beam propagates toward a sample, and a CCD camera records the diffraction pattern for each wavelength by turning the lasers on and off sequentially. (b) Schematic of the Fresnel diffraction geometry used in the microscope. The diverging beam from the SMF is transmitted through an object onto a CCD. The beam divergence introduces a magnification factor in the microscope. (c) Picture of the imaging setup, showing the fiber output, the CCD camera, and the dish containing a coverslip with cells.

(FOV) as determined from the CCD size and number of pixels is then 1.1×0.87 mm, although in practice the illuminated area is the limiting factor due to the required magnification factor (see below), which restricts the FOV to a slightly smaller area.

Fresnel diffraction patterns are recorded at the three different wavelengths with an exposure time of 0.8 ms per image. Near-infrared wavelengths are used to minimize absorption and scattering by biological samples, while still having sufficient photon energy record the diffraction patterns with a Si-based CCD detector. Also, the dispersion of water and biological material is low in the near-infrared, so that it does not affect the phase retrieval. If this is not the case (e.g., when using visible wavelengths), the refractive index change can be explicitly incorporated into the phase retrieval algorithm through, e.g., known Sellmeier equations of water and/or bulk protein.

In the Fresnel diffraction regime, the pixel size of the CCD camera may be a limiting factor for the resolution, as this limits the resolution at which the diffraction pattern is sampled and therefore reconstructed. To remove this limitation, we introduce a magnification by illuminating the sample with a strongly diverging wave, which is readily obtained by using the output beam of a single-mode optical fiber, as shown in Fig. 1(b). The magnification of the recorded diffraction pattern can be controlled by adjusting the distance between the fiber output and the sample, while keeping the sample-camera distance fixed. In this geometry, the effective pixel size at the

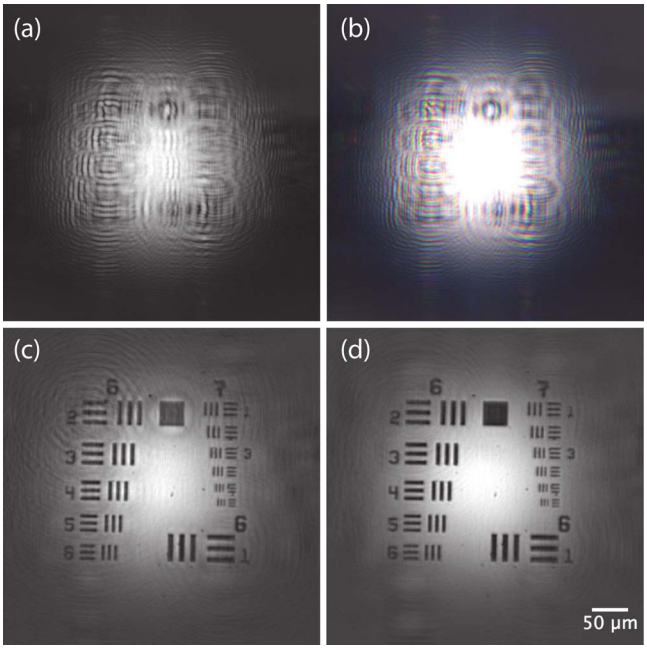

Fig. 2. (a) Diffraction pattern of a USAF1951 resolution test target at 785 nm wavelength (logarithmic intensity scale). (b) Overlay of three diffraction patterns of the same object (log scale), recorded at 685 nm (blue), 785 nm (green), and 940 nm (red). (c) Retrieved image after 30 iterations of the multiwavelength phase retrieval algorithm and backpropagation to the object plane. Two diffraction patterns at 685 and 785 nm are used as input. (d) Retrieved image after the same phase retrieval procedure, using three diffraction patterns (wavelengths 685, 785, and 940 nm) as input.

object plane is given by the CCD pixel size divided by the magnification. In the geometry used to image the USAF target the magnification is 7.5, and the resulting pixel size at the object plane is 0.6 μm. Advantages of this approach compared to other pixel-super-resolution methods [4,6] are that light source movement is not needed, and only three diffraction patterns are required to produce a high-resolution image.

Figure 2(a) shows a diffraction pattern of the USAF1951 test target at a wavelength of 785 nm. Similar diffraction patterns are recorded at the other two wavelengths. To highlight the wavelength dependence of the Fresnel diffraction, an overlay of the diffraction patterns at the three different wavelengths is displayed in Fig. 2(b). These images form the basis for the multiwavelength phase retrieval algorithm. In principle, only two diffraction patterns are required for the algorithm to work. That this is indeed the case is shown in Fig. 2(c), where a clear image of the test target is obtained, although some residual interferences can be seen in the reconstruction. The use of more than two wavelengths improves the reconstruction further, as noise is averaged over more measurements and small artefacts due to camera read noise are at different image positions for different wavelengths. This is highlighted by Fig. 2(d), displaying a reconstruction using diffraction patterns at all three wavelengths, in which the imperfections that remained in the two-wavelength case are fully removed. By analyzing Fig. 2(d), we find that a transverse resolution of 1.8 μm is achieved, which is 1.5× the diffraction limit and 2.5× smaller than the camera pixel size. The algorithm converged within 30 iterations, which takes about 1 min of processing time on a standard desktop computer when using 1936 × 1456 pixel images. However, the required calculations are well suited for parallel processing: a first implementation of the algorithm on a graphical processing unit achieved around 100 iterations per second, indicating that an update rate of several hertz is achievable with a fully integrated data acquisition and processing system.

To demonstrate the capabilities of our multiwavelength lensless microscope for live cell imaging, we perform imaging experiments on mouse hippocampal neurons, which have been cultured on top of a layer of rat astrocytes on a coverslip. A typical diffraction pattern at 940 nm wavelength is shown in Fig. 3(a). Both an intensity and a phase image are obtained after 30 iterations of the algorithm, which are shown in Figs. 3(b) and 3(c), respectively. Cells can be considered to be phase objects due to their transparency, which makes phase contrast microscopy essential for obtaining high-contrast images. This is illustrated by a comparison between the

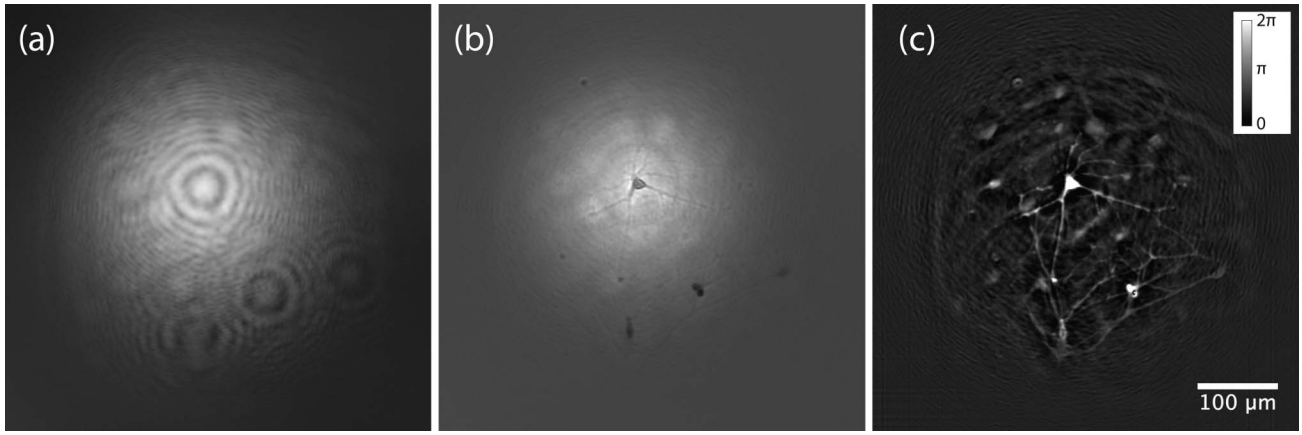

Fig. 3. (a) Diffraction pattern (logarithmic intensity scale) of a sample of live neurons grown on astrocytes, recorded at 940 nm wavelength. (b) Reconstructed intensity image at the object plane, using diffraction patterns at three wavelengths. (c) Reconstructed phase image of the sample, clearly showing the neurons. The scale bar shows the measured phase shift in radians.

intensity image in Fig. 3(b), in which a few cell bodies and dendrites can be identified, and the phase image in Fig. 3(c), which clearly shows many fine details of the cells and their network of dendrites. In addition, the phase image also provides a clear view of the astrocytes on which the neurons are cultured. The ability to retrieve a quantitative phase map enables a measurement of the optical path length through the cells, from which additional information on the height profile of the cells can be obtained [19,20].

In summary, we have developed a lensless quantitative phase contrast microscope, which exploits diffraction patterns recorded at multiple wavelengths to enable robust image reconstruction without the need for moving parts. Quantitative phase images with <2 μm transverse resolution are obtained using an iterative phase retrieval algorithm, requiring diffraction patterns at only three different wavelengths as input. The setup consists of a fully fiber-integrated light source and a CCD camera, and allows a tunable magnification factor through the use of a divergent illumination geometry. We have verified the potential of our setup for live cell imaging applications by recording high-resolution phase contrast images of living cultured neurons in solution. Further advances are expected through the implementation of a camera with a smaller pixel size, which relaxes the magnification requirements for achieving micrometer resolution, and allows a higher FOV at a given resolution. Our system has favorable properties in terms of compactness and cost-effectiveness compared to lens-based microscopes with similar capabilities. We therefore anticipate that our system may become a useful alternative in applications where quantitative phase imaging is important, such as cell biology or surface profiling.

We thank Dr. R. F. G. Toonen and D. Schut for providing the neuron samples, and M. Stoffels for assistance with the algorithm implementation. S.W. acknowledges support from the Netherlands Organization for Scientific Research (NWO) through Veni grant no. 680-47-402. This work is partly financed by an NWO-groot investment grant.

References

1. W. Denk, J. H. Strickler, and W. W. Webb, Science **248**, 73 (1990).
2. S. W. Hell, Science **316**, 1153 (2007).
3. P. Kner, B. B. Chhun, E. R. Griffis, L. Winoto, and M. G. L. Gustafsson, Nat. Methods **6**, 339 (2009).
4. G. Zheng, S. A. Lee, Y. Antebi, M. B. Elowitz, and C. Yang, Proc. Natl. Acad. Sci. USA **108**, 16889 (2011).
5. W. Xu, M. H. Jericho, I. A. Meinertzhagen, and H. J. Kreuzer, Proc. Natl. Acad. Sci. USA **98**, 11301 (2001).
6. W. Bishara, T.-W. Su, A. F. Coskun, and A. Ozcan, Opt. Express **18**, 11181 (2010).
7. J. R. Fienup, J. Opt. Soc. Am. A **4**, 118 (1987).
8. S. Marchesini, Rev. Sci. Instrum. **78**, 011301 (2007).
9. Y. M. Bruck and L. G. Sodin, Opt. Commun. **30**, 304 (1979).
10. L. J. Allen and M. P. Oxley, Opt. Commun. **199**, 65 (2001).
11. Y. Zhang, G. Pedrini, W. Osten, and H. J. Tiziani, Opt. Express **11**, 3234 (2003).
12. A. Greenbaum and A. Ozcan, Opt. Express **20**, 3129 (2012).
13. H. M. L. Faulkner and J. M. Rodenburg, Phys. Rev. Lett. **93**, 023903 (2004).
14. J. M. Rodenburg, A. C. Hurst, A. G. Cullis, B. R. Dobson, F. Pfeiffer, O. Bunk, C. David, K. Jefimovs, and I. Johnson, Phys. Rev. Lett. **98**, 034801 (2007).
15. A. M. Maiden, J. M. Rodenburg, and M. J. Humphry, Opt. Lett. **35**, 2585 (2010).
16. A. Jesacher, C. Roider, and M. Ritsch-Marte, Opt. Express **21**, 11150 (2013).
17. S. Witte, V. T. Tenner, D. W. E. Noom, and K. S. E. Eikema, "Ultra-broadband extreme-ultraviolet lensless imaging of extended complex structures," arXiv:1302.6064 (2013).
18. J. W. Goodman, *Introduction to Fourier Optics*, 3rd ed. (Roberts & Company 2005).
19. B. Rappaz, P. Marquet, E. Cuche, Y. Emery, C. Depeursinge, and P. J. Magistretti, Opt. Express **13**, 9361 (2005).
20. S. Witte, A. Plauşka, M. C. Ridder, L. van Berge, H. D. Mansvelder, and M. L. Groot, Biomed. Opt. Express **3**, 2184 (2012).